Single-device offset-free magnetic field sensing with tunable sensitivity and linear range based on spin-orbit torques

Sabri Koraltan[1,2,*] Christin Schmitt,[3] Florian Bruckner,[1] Claas Abert,[1,4] Klemens Prügl,[5]
Michael Kirsch,[5] Rahul Gupta,[3] Sebastian Zeilinger,[1,6] Joshua M. Salazar-Mejía,[1,2]
Milan Agrawal,[7] Johannes Güttinger,[6] Armin Satz,[6] Gerhard Jakob,[3] Mathias Kläui,[3] and
Dieter Suess[1,4]

[1]*Physics of Functional Materials, Faculty of Physics, University of Vienna, Vienna, Austria*
[2]*Vienna Doctoral School in Physics, University of Vienna, Vienna, Austria*
[3]*Institute of Physics, Johannes Gutenberg University Mainz, Mainz 55099, Germany*
[4]*Research Platform MMM Mathematics-Magnetism-Materials, University of Vienna, Vienna, Austria*
[5]*Infineon Technologies AG, Regensburg, Germany*
[6]*Infineon Technologies AG, Villach, Austria*
[7]*Infineon Technologies AG, Munich, Germany*

We propose a novel device concept that uses spin-orbit torques to realize a magnetic field sensor, where we eliminate the sensor offset using a differential measurement concept. We derive a simple analytical formulation for the sensor signal and demonstrate its validity with numerical investigations using macrospin simulations. The sensitivity and the measurable linear sensing range in the proposed concept can be tuned by varying the effective magnetic anisotropy or the magnitude of the injected currents. We show that undesired perturbation fields normal to the sensitive direction preserve the zero-offset property and only slightly modulate the sensitivity of the proposed sensor. Higher harmonic voltage analysis on a Hall cross experimentally confirms the linearity and tunability via current strength. Additionally, the sensor exhibits a nonvanishing offset in the experiment, which we mostly attribute to the anomalous Nernst effect.

I. INTRODUCTION

Spintronics has been a very active field of research since the discovery of the giant magnetoresistive effect [1,2]. With the ability to control the magnetization of magnetic materials using spin-polarized currents [3–5], new possibilities have emerged for spintronic devices [6–9]. Spin-orbit-torque-induced magnetization switching processes have been proven to be ultrafast and energy efficient [10–14]. Furthermore, spin currents have been used to propagate chiral objects such as domain walls [15] or skyrmions [16–19]. A newly developed topic in this area is the use of spin-orbit torque (SOT) for magnetic field sensing [8,20–22].

Accurate sensors for magnetic field measurements [23] are very important for various applications, such as biosensors and biochips for medical use [24], read heads for magnetic recording devices [25], or for speed wheel sensors with vortex sensors used in the automotive industry [26]. Conventional magnetoresistive field sensors rely on the response of a rather soft magnetic layer to the external

field. An additional hard magnetic layer that is insensitive to changes in the external field acts as a reference system, introducing a field-dependent magnetoresistivity. The linear regime for these systems can be tuned to various field ranges by adjusting the material properties or geometry of the soft magnetic layer.

To obtain a sensor output around zero, conventional magnetoresistive sensors are operated in Wheatstone bridge configurations. However, this leads to zero-field offsets due to fabrication tolerances of different elements and thermal drift within and between different elements.

Alternative approaches have emerged over the past years, where instead of exploiting magnetoresistive effects, current is sent through the magnetic layers directly and transverse voltages are measured. The changes in the magnetization cause this transverse voltage, which is called the anomalous Hall voltage. Anomalous Hall effect (AHE) sensors have been proven to be ultrasensitive and accurate for sensing low magnetic fields [27–29]. Note that, due to Ohm's law, magnetoresistance measurements operated without a Wheatstone bridge exhibit an offset at vanishing fields. Thus, it is difficult to obtain accurate measurement results for small external fields without proper calibration.

---

*sabri.koraltan@univie.ac.at

In commercial tunnel magnetoresistive (TMR) sensors this offset is around 1 mT, and thus the limiting factor for absolute field sensing. Therefore, it is a key challenge in magnetic field measurement applications to reduce or eliminate the zero-field offset. There are several designs in which the offset can be reduced or almost eliminated. These solutions are based on spinning current techniques for Hall sensors or still use Wheatstone bridges where four distinct magnetic stacks are required to eliminate the offset [20]. Recently, a three-dimensional (3D) magnetic field sensor using SOTs was reported [21], where a change in the position of the domain wall leads to a sensor signal. However, in both cases, the linear range is extremely small.

In this work, we propose a sensor concept for magnetic field measurements that takes advantage of the symmetric nature of SOT to eliminate the sensing offset. Using micromagnetic simulations, we demonstrate that a differential measurement method using SOT eliminates the offset error. We reveal how increasing the amplitude of the injected current can be used to tune the sensor's sensitivity, whereas higher perpendicular magnetic anisotropies enhance the linear range. The robustness of the measurement scheme is tested by investigating the role of perturbation fields normal to the sensitive direction on the offset and sensitivity. The proposed concept is experimentally tested on a Hall cross stack, where a Ta layer is used as the heavy metal layer and spin polarizer and a thin film of Co-Fe-B is deposited on top as the magnetic layer. Second harmonics measurements are performed to obtain the linear sensor signal via the anomalous Hall effect.

II. CONCEPT

The proposed sensor concept is based on a Hall cross with a heavy metal (HM) underlayer and a ferromagnetic (FM) top layer with perpendicular magnetic anisotropy (PMA); see Fig. 1. Subject to an electric current in the $\pm x$ direction, the spin Hall effect [30] in the HM layer leads to a spin current with polarization in the $\mp y$ direction flowing into the magnetic layer. This leads to a spin torque called the spin-orbit torque [5].

If an in-plane current is injected through the HM layer, a transverse voltage can be measured using the AHE. If negligible SOT currents are applied, changes in magnetization can be measured caused by externally applied magnetic fields. When the magnitude of the charge current increases, the SOT scales accordingly. The higher SOT torques we discuss later will change the magnetization state. In this case, an anomalous Hall voltage modulated by SOT can be measured. Therefore, the proposed sensing concept is an anomalous Hall voltage sensor enabled by SOT. For a vanishing external field and charge current, the equilibrium magnetization in the magnetic layer is perfectly aligned out of the plane (OOP) due to PMA. The response of the magnetic system to the spin-orbit torque is perfectly symmetric [31] when changing the sign of the electric current in the heavy metal layer; see Fig. 1(a). However, if an external field is applied, the equilibrium position of the magnetization is tilted, and the AHE response to the SOT becomes asymmetric; see Fig. 1(b).

The main idea of the proposed sensing principle is to perform differential measurements with direct currents applied subsequently in the opposite direction to exploit
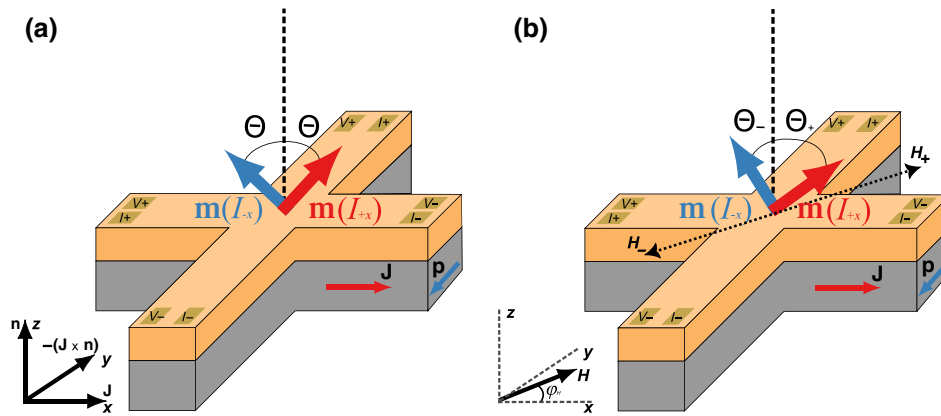

FIG. 1.   Schematic illustration of the zero-offset magnetic field sensor. The ferromagnetic layer (orange, in experiment $Co_{60}Fe_{20}B_{60}$) is situated on top of the heavy metal layer (gray, in experiment Ta) that acts as a spin polarizer. Upon application of a charge current through the HM layer $\mathbf{J}$ a spin-polarized current flows along $\mathbf{n}$ into the FM layer with polarization $\mathbf{p} = (\mathbf{J} \times \mathbf{n})$. The behavior of the single-domain OOP magnetization is illustrated first in (a) with a vanishing external field, where the initial magnetization $\mathbf{m}_0$ is now tilted to $\mathbf{m}(I_{+x})$ for a positive charge current and to $\mathbf{m}(I_{-x})$ for a negative charge current. The angle of deviation Θ is the same for both current directions. After tilting, the magnetization will have both x and y components in addition to the z component. The change induced by an external field applied in the plane is illustrated in (b), where the presence of the external field disturbs the symmetry of the SOT. The magnetic field is applied at an angle ϕ_H that defines the sensitive direction (x-y plane), where $\tan\phi_H = H_{dl}/H_{fl}$. The resulting angles Θ_+ and Θ_- now differ in magnitude.

this symmetry and eliminate the offset for the zero-field case.

To better highlight the advantages of the proposed sensing concept, we have a look at the recent advances in AHE-, SOT-, or spin-Hall-magnetoresistance- (SMR) enabled sensors that make use of a similar approach. The aim was to use either an HM-FM bilayer or a Co-Fe-B layer to generate a linear response to an externally applied magnetic field. Table I summarizes recent relevant work in which magnetic field sensors have been realized experimentally. Commercially available Hall sensors from Allegro [32] have a high sensitivity and linear range in their final products. The current dc offset is below 1 mT. Infineon technologies offer a TMR sensor based on Ref. [26] to sense B_x fields. In this case, the TMR enables a very high sensitivity and also a good linear range. However, there is still a dc offset of 1 mT, which limits the sensing resolution. Zhu *et al.* [27] considered an in-plane magnetized Co-Fe-B layer deposited on Ta and measured the change in transverse resistance via the AHE when the low charge current is sent directly through the magnetic layer. Thus, a highly sensitive AHE sensor can be achieved with a linear range of approximately ±1 mT and a maximum sensitivity of approximately 237.6 Ω/T. Peng *et al.* [28] showed that, compared to regular Ta/Co-Fe-B/MgO trilayers, the insertion of an additional ultrathin Gd or Hf layer between Ta and Co-Fe-B can increase both the linear range and the sensitivity to ±3.5 mT and 10 040 Ω/T, respectively. Note that the insertion of Hf leads to an even higher sensitivity of 28 282 Ω/T, but reduces the linear range to 1 mT. Xu *et al.* [20] chose a different approach, where the HM-FM layer was composed of Pt and NiFe ellipses, which are built in a Wheatstone bridge configuration. Similarly to our approach, the charge current is sent through the HM layer, which generates a SOT that acts on the in-plane magnetization of NiFe ellipses. Note that the sensor signal is then measured as the average dc contribution after applying an alternating charge current with subkilohertz frequencies.

The idea of a SOT sensor using a perpendicularly magnetized sample was demonstrated by Li *et al.* [21], where they used a thin Co-Fe-B layer on a large Hall cross to generate a long domain wall in the center of the cross. When an in-plane current is applied through the HM layer (Ta), the magnetization experiences a SOT. With the applied external field, the domain wall position changes, leading to a symmetric change in the measured AHE voltage. The measurable linear range is again limited to only ±1 mT, while the sensitivity to measure the x component is 205 Ω/T. Since this approach allows 3D sensing, it should be noted that the OOP component can be measured with a much higher sensitivity of about 1845 Ω/T, but with a lower linear range of 0.4 mT.

Although the summarized academic cases show very high sensitivities, the measurable linear ranges remain below 3.5 mT. Thus, a sensing concept with a higher measurable linear range, and eliminated dc offset is a crucial advance in spin-orbitronic devices for sensing magnetic fields, as most applications such as position and speed wheel sensors in the automotive industries require larger measurable ranges.

III. MODELING

In order to verify the feasibility of the proposed concept, we perform a series of macrospin simulations in which the SOT interactions with the magnetization are described by the Landau-Lifshitz-Gilbert (LLG) equation [33,34]

$$\partial_t \mathbf{m} = -\gamma \mathbf{m} \times \mathbf{H}^{\text{eff}} + \alpha \mathbf{m} \times \partial_t \mathbf{m} + \mathbf{T}_{\text{damp}} + \mathbf{T}_{\text{field}}, \quad (1)$$

where γ is the gyromagnetic ratio, $\mathbf{H}^{\text{eff}}$ is the effective field of the FM layer, and α is the Gilbert damping coefficient. The LLG equation is extended by two additional current-induced torques [34–36]

$$\mathbf{T}_{\text{damp}} = \eta_{\text{damp}} \frac{j_e \gamma \hbar}{2e\mu_0 t M_s} \mathbf{m} \times (\mathbf{m} \times \mathbf{p}) \quad (2)$$

TABLE I.   Comparison of recent sensor concepts which use FM/HM layers or anomalous Hall effect to read.

	Type	Component	Linear range (mT)	Sensitivity (Ω/T)	Linear range × sensitivity (Ω)	Offset (mT)
Allegro [32]	Hall	B_z	±37.5	4444.44	166.67	0.62
Infineon	TMR	B_x	±35	90 000	3150	1
Zhu *et al.* [27]	AHE	B_z	±1	237.6	0.2376	⋯
Peng *et al.* [28]	AHE	B_z	±3.5	10 040	35	⋯
Xu *et al.* [20]	SOT SMR	B_y	±0.05	3464	0.17	⋯
Li *et al.* [21]	SOT AHE	B_x	±1	205	0.205	⋯
Li *et al.* [21]	SOT AHE	B_y	±1	282	0.282	⋯
Li *et al.* [21]	SOT AHE	B_z	±0.4	1845	0.738	⋯
This work, $H_k = 200$ and $j_e = 1$ MAcm^{-2}	SOT AHE	$B_{x,y}$	±180	0.017	0.003	0
This work, $H_k = 200$ and $j_e = 50$ MAcm^{-2}	SOT AHE	$B_{x,y}$	±15	1.32	0.2	0

and

$$\mathbf{T}_{\text{field}} = \eta_{\text{field}} \frac{j_e \gamma \hbar}{2e\mu_0 t M_s} \mathbf{m} \times \mathbf{p}, \tag{3}$$

with $\hbar$ being the reduced Planck constant, e being the elementary charge, and μ_0 being the vacuum permeability. The magnitudes of the two torques depend on the charge current density j_e applied in the heavy metal layer, on the parameters of the ferromagnetic layer, i.e. saturation magnetization M_s, thickness t, and on the dimensionless SOT coefficients η_{damp} and η_{field}.

Equation (1) can then be written as

$$\partial_t \mathbf{m} = -\gamma \mathbf{m} \times (\mathbf{H}^{\text{eff}} - H_{\text{dl}} \mathbf{m} \times \mathbf{p} - H_{\text{fl}} \mathbf{p}) + \alpha \mathbf{m} \times \partial_t \mathbf{m}, \tag{4}$$

where

$$H_{\text{dl}} = \frac{j_e \hbar}{2e\mu_0 t M_s} \cdot \eta_{\text{dl}} \tag{5}$$

and

$$H_{\text{fl}} = \frac{j_e \hbar}{2e\mu_0 t M_s} \cdot \eta_{\text{fl}} \tag{6}$$

are the magnitudes of the current-induced dampinglike and fieldlike torques.

A. First-order analytical approximation

The magnetization dynamics of a perpendicularly magnetized system can be described by macrospin simulations where Eq. (4) is solved numerically or by employing an analytical approach similar to that proposed by Hayashi *et al.* [37]. Here, we derive a simpler first-order approximation based on the Stoner-Wolfarth formalism.

Let us now assume that the ferromagnetic layer is homogeneously magnetized along the [001] direction, $m_0 = (0, 0, 1)^{\text{T}}$. When a homogeneous magnetic field is applied in the x-y plane, the effective field H^{eff} is given solely by the contribution of the anisotropy and Zeeman energies [34] as

$$H^{\text{eff}} = \begin{pmatrix} H_x \\ H_y \\ H_k \end{pmatrix}, \tag{7}$$

where H_x and H_y are the components of the applied in-plane field, and H_k is the effective anisotropy field.

To account for the spin-orbit torque, the effective field must be complemented according to Eq. (4). In the case of a spin polarization in the y direction, the fieldlike torque only contributes via the y component of the effective field given by

$$H_y^{\text{eff}} = H_y - p_y \cdot H_{\text{fl}}, \tag{8}$$

whereas the dampinglike torque contributes to the x component as

$$H_x^{\text{eff}} = H_x - (\mathbf{m} \times \mathbf{p})_x \cdot H_{\text{dl}}. \tag{9}$$

The magnitude of the external field applied along the sensitive direction and the SOT fields is then given by

$$H_\parallel = \sqrt{(H_x^{\text{eff}})^2 + (H_y^{\text{eff}})^2}. \tag{10}$$

According to the hard-axis approximation of the Stoner-Wohlfarth model, the parallel component of the magnetization is given as

$$m_\parallel = \frac{H_\parallel}{H_k}, \tag{11}$$

where H_k is the anisotropy field.

The z component of magnetization can then be simply obtained from the unit magnetization constraint where

$$m_z = \pm\sqrt{1 - m_\parallel^2}, \tag{12}$$

with the sign depending on the initial sign of m_z.

Consider now that we apply a dc current I_0 along the $+x$ direction. For simplicity, we refer to this current as I_{+x}. If the current is applied along the $-x$ direction, $I_{-x} = -I_0$. As explained in Sec. II, this leads to a change in magnetization, with the new magnetization state being $m_z(I_{+x})$, which is proportional to the anomalous Hall resistance, where

$$R_{xy}(I_{+x}) = \Delta R_{\text{AHE}} m_z(I_{+x}) \tag{13}$$

with ΔR_{AHE} the anomalous Hall coefficient. Thus, we obtain the Hall voltage $V_{xy}(I_{+x}) = \Delta R_{\text{AHE}} m_z(I_{+x}) I_{+x}$.

The sensor signal can be obtained as the difference in measured resistances

$$S = R_{xy}(I_{+x}) - R_{xy}(I_{-x}), \tag{14}$$

or as a sum of measured AHE voltages:

$$S_{xy} = V_{xy}(I_{+x}) + V_{xy}(I_{-x}). \tag{15}$$

The linear sensor signal S can be derived directly from Eq. (12). Let us now assume the most general case, where both SOT coefficients are included and a field with components H_x and H_y is applied to be aligned with the sensitive direction. We can then write

$$V_{xy}(I_{+x}) = \pm \Delta R_{\text{AHE}} I_{+x} \sqrt{1 - \frac{(H_x \mp H_{\text{dl}})^2 + (H_y + H_{\text{fl}})^2}{H_k^2}}. \tag{16}$$

After expanding Eq. (16) in a Taylor series at $H_x = 0$ and $H_y = 0$ and summing up the resulting voltages given in

Eqs. (A5) in Appendix A according to Eq. (15), one obtains the simplified analytical approximation of the sensor signal where

$$S_{xy} = 2\Delta R_{\mathrm{AHE}} I_0 \left(H_{\mathrm{dl}} \frac{H_x}{H_k{}^2} \mp H_{\mathrm{fl}} \frac{H_y}{H_k{}^2} \right)$$
$$+ \mathcal{O}[H_x]^2 + \mathcal{O}[H_y]^2. \qquad (17)$$

The field components H_x and H_y can be written as $H_x = H \cos\phi_H$ and $H_y = H \sin\phi_H$, respectively. Therefore, the total sensor signal becomes

$$S_{xy} = 2\Delta R_{\mathrm{AHE}} I_0 \frac{H(H_{\mathrm{dl}} \cos\phi_H \mp H_{\mathrm{fl}} \sin\phi_H)}{H_k^2}$$
$$+ \mathcal{O}[H_x]^2 + \mathcal{O}[H_y]^2. \qquad (18)$$

B. Equivalency to higher harmonic voltage measurements

For systems where very low signals are expected or highly accurate measurements are desired, a higher harmonic voltage analysis (HHVA) can be performed [14,31, 37,38]. In this case, one applies an ac current instead of performing two subsequent measurements with opposite currents. The applied frequencies are generally in the hertz range.

Consider again the perpendicularly magnetized system, where the magnetization is modulated by SOTs. Upon application of the current $I(t) = I_0 \sin(\omega t)$, the magnetization component m_z, and thus R_{xy}, oscillates with angular frequency 2ω. The time-dependent Hall voltage can be expressed as

$$V_{xy}(t) = R_{xy} I(t). \qquad (19)$$

Substituting R_{xy} with the temporal evolution of Eq. (13) one obtains

$$V_{xy}(t) = \Delta R_{\mathrm{AHE}} I(t) m_z(t), \qquad (20)$$

which can be further completed with the first-order approximation for the z component of the magnetization:

$$V_{xy}(t) = \pm \Delta R_{\mathrm{AHE}} I_0 \sin(\omega t)$$
$$\times \sqrt{1 - \frac{(H_x \mp H_{\mathrm{dl}}(t))^2 + (H_y + H_{\mathrm{fl}}(t))^2}{H_k^2}}. \qquad (21)$$

As described in Appendix B, one can then perform a second-order Fourier series expansion of Eq. (21) with

respect to ωt, and arrange the terms accordingly to obtain

$$V_{xy}(t) = \frac{I_0 \Delta R_{\mathrm{AHE}}(H_{\mathrm{dl}} H_x \mp H_{\mathrm{fl}} H_y)}{2H_k^2}$$
$$\mp \frac{I_0 \Delta R_{\mathrm{AHE}}(3(H_{\mathrm{dl}}^2 + H_{\mathrm{fl}}^2) - 16 H_k^2 + 4(H_x^2 + H_y^2))}{8 H_k^2}$$
$$\times \sin(\omega t)$$
$$- \frac{I_0 \Delta R_{\mathrm{AHE}}(H_{\mathrm{dl}} H_x \mp H_{\mathrm{fl}} H_y)}{2H_k^2} \cos(2\omega t). \qquad (22)$$

Based on the common higher harmonics voltage analysis, where the time-dependent AHE voltage is given as

$$V_{xy}(t) = V_0 + V_\omega \sin(\omega t) + V_{2\omega} \cos(2\omega t), \qquad (23)$$

one can express the second harmonic voltage as

$$V_{2\omega} = \frac{I_0 \Delta R_{\mathrm{AHE}}(H_{\mathrm{dl}} H_x \mp H_{\mathrm{fl}} H_y)}{2H_k^2}, \qquad (24)$$

which differs from our sensor signal approximation in Eq. (18) by only a constant factor.

Thus, one can measure the sensor signal either by the sum of AHE voltages for positive and negative currents, by applying an ac current and measuring the dc contribution, or by measuring the field dependence of the second harmonic voltage using HHVA, e.g., with a lock-in amplifier.

C. Micromagnetic simulations

In order to check the accuracy of the analytical model, we additionally perform fully dynamical LLG simulations. For the sake of simplicity, we use a macrospin approximation to simulate the magnetic layer using the micromagnetic simulation software `magnum.np` [39]. For the effective field, we consider only the effective anisotropy field and the external field. The effect of the demagnetization field is considered in terms of a contribution to the anisotropy field. As material parameters, we have chosen saturation magnetization $\mu_0 M_s = 1.2$ T and Gilbert damping constant $\alpha = 1$ as suitable material parameters for a Ta/Co-Fe-B/MgO system [5,40]. Note that the saturation magnetization and effective anisotropy strongly depend on the thickness of the FM layer. If the Ta/Co-Fe-B/MgO trilayer is annealed in an external magnetic field and (or) the annealing temperatures are varied, the saturation magnetizations [40] can be tuned. Typically, $\mu_0 M_s$ varies between 0.7 and 1.5 T. However, injecting a charge current that is too large will cause Joule heating, which will reduce not only saturation magnetization but also the effective PMA. As we are interested only in the magnetic equilibrium states, we are using the high Gilbert damping parameter $\alpha = 1$. Since the thickness of the magnetic layer is

crucial for the strengths of current-induced torques, we assume everywhere a thickness of $t = 1$ nm, and for the thickness of the HM layer, we choose $t_{HM} = 6$ nm. To obtain the voltage from the magnetization component m_z, we consider a cross section $A = L \times t = 10 \ \mu\text{m} \times 7$ nm to calculate the applied current from the magnitude of the applied current density j_e, and assume that $\Delta R_{AHE} = 0.15 \ \Omega$.

IV. EXPERIMENTAL METHODS

Our numerical investigations are accompanied by experimental validations, where a SOT stack consisting of an HM layer, Ta, and an FM layer, Co-Fe-B is used. Because of the equivalence shown in Sec. III B, we measure the second harmonic voltage with a lock-in technique to investigate the field dependency of the sensor signal.

A. Sample fabrication

The SOT structure was grown on an 8-in. silicon wafer using a Singulus Rotaris tool. Before the film stack was deposited, the wafers received an aluminum metallization layer to contact the SOT structure from the bottom. The connection of the SOT structure to the aluminum metal layer through an insulation layer SiO_2 was made with tungsten vias. To have a smooth surface before depositing the SOT film stack, a chemical mechanical polish was carried out. The film stack consisted of $Ta[6 \text{ nm}]/C_{60}Fe_{20}B_{20}[1 \text{ nm}]/MgO[1.5 \text{ nm}]/Ta[5 \text{ nm}]$. It was grown without vacuum brake by physical vapor deposition with a base pressure $< 5 \times 10^{-9}$ torr. The sputter gas used was argon for all layers. Metal deposition was performed in the dc sputtering mode, and MgO deposition was performed in the rf mode. After deposition, the wafers were annealed for 2 h at a temperature of $280 \,^\circ$C under vacuum. Patterning of the SOT structure can be done by reactive ion etching with chlorine or by ion beam etching, whereas the latter needs an additional hard mask. The Hall bars used in this study were patterned from the films using conventional optical lithography and Ar ion etching. To prevent the SOT structure from corrosion, a passivation layer was deposited. Note that further encapsulation by aluminum-filled vias surrounding and metallization layers on top of the SOT structure leads to better heat dissipation. Finally, the pads were released by opening the passivation layer. Standard separation techniques (mechanical dicing) were used.

B. Second harmonic measurements

The harmonic voltages are measured using a standard second harmonic lock-in amplifier detection-based technique, where we utilize a vector magnet to apply the magnetic field in different directions. We used standard wire bonding to connect the Hall bar device with the sample

holder. The Hall bar was connected to 50-Ω resistance in series to measure the input sinusoidal current during measurement. The schematic is shown in Fig. 1(a). Before harmonic measurements, the Hall bar device was presaturated along the $\pm z$ direction. We applied a sinusoidal voltage with constant amplitude (V_{in}) using a lock-in amplifier (model number HF2LI by Zurich instrument) to the Hall bar device with a reference frequency of 13.7 Hz. Two other lock-in amplifiers (model numbers 7265 and 7225) were used to measure the first and second harmonic voltages in phase simultaneously.

V. RESULTS

A. Role of SOT coefficients

We begin our numerical investigation with a thorough investigation of the role of the SOT coefficients on the equilibrium states, as this will define the sensitive direction of our magnetic field sensor. By using a macrospin approximation as explained in Sec. III C, we vary the field-like and dampinglike coefficients η_{damp} and η_{field} that will alter the strengths of the torques exerted on the magnetization. For this purpose, we use an effective anisotropy field $\mu_0 H_k = 200$ mT, and apply a SOT current density of magnitude $j_e = 1 \ \text{MAcm}^{-2}$.

In Fig. 2, one can see the influence of the SOT coefficients on the equilibrium magnetization state. As expected and briefly mentioned during the derivation of the first-order analytical approximation, the variation of η_{dl} only changes the x component of the magnetization; see Fig. 2(a), while the variation of η_{fl} modulates m_y, as illustrated in Fig. 2(b). Both torques contribute to the inclination of magnetization in a symmetric way, as shown in Fig. 2(c). In principle, the choice of the HM layer will lead to a specific pair of η_{damp} and η_{field} [5], which in return will then modulate the sensitive direction of the sensor. The strengths of the SOT coefficients can then be determined by measuring the first and second harmonic voltages and applying the Hayashi method for perpendicularly magnetized systems [37]. If the planar Hall effect is negligible, the expressions for V_ω and $V_{2\omega}$ given in Eq. (22) can also be used. Alternative techniques such as spin-torque ferromagnetic resonance [5] exist that lead to precise determination of the dampinglike coefficient.

We have chosen $\eta_{damp} = -0.4$ and $\eta_{field} = 0.5$ for all future investigations, so that the sensitive direction is slightly away from the [110] axis. The sensitive axis can also be calculated simply from the ratio of the two current-induced torques given in Eqs. (5) and (6) where $\tan \phi_H = H_{dl}/H_{fl}$. Note that the signs of the SOT coefficients depend on their definition in the LLG equation. In our case, a positive fieldlike coefficient means that the torque acts parallel to the Oersted field that is generated by the current flow in the SOT stack [5].
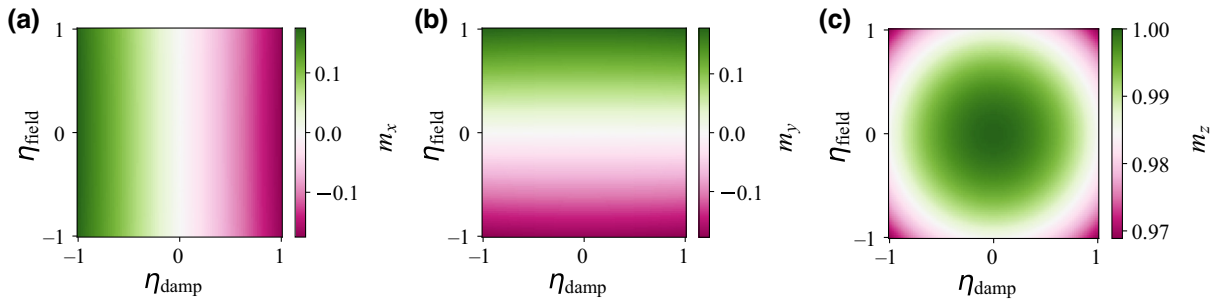
FIG. 2. Dependence of the SOT coefficients on the equilibrium magnetization when a SOT current is applied to a macrospin. In (a) we see that the dampinglike torque modulates the x component. From (b) we observe that the fieldlike coefficient modulates the y component of the magnetization, whereas from (c) we learn that both torques contribute to the modulation of the z component of the magnetization.

B. Operation as a linear magnetic field sensor

Using our macrospin simulations, we subsequently apply the charge current in opposite directions, where $j_e = 1$ MAcm^{-2} and $\mu_0 H_k = 200$ mT. Now, we apply a magnetic field along the obtained sensitive axis $\mathbf{H}_\parallel$. Figure 3(a) shows the evolution of V_{xy} as the response of magnetization to the applied field. As in the simplified analytical model [Eq. (16), lines], the macrospin simulations (filled symbols) yield a parabolic dependence of V_{xy} from the measured field $H_\parallel$. For opposite charge currents, the magnetization is modulated symmetrically around the vanishing magnetic field. If the applied magnetic field exceeds a specific threshold then the magnetization changes sign. Note that the simulated voltages are calculated by assuming a $\Delta R_{AHE} = 0.15$ Ω. Changing this value with experimentally measured values will affect the quantitative analysis of the relevant sensing parameters. Thus, only a qualitative analysis between numerical results and experimental studies can be considered if ΔR_{AHE} is not chosen realistically.

Using the proposed differential measurement, we obtain the sensor signal shown in Fig. 3(b). The sensor signal is obtained as the sum of Hall voltages. These signals are obtained from macrospin simulations (red), from Eq. (15) (blue), and from Eq. (18) (green line). A high linear range is observed, which is slightly smaller than the anisotropy field. Figure 3(c) shows an enlarged view of the relevant section from (b), which shows good agreement between all three curves in the limit of small fields. The sensitivity of the sensing device, given by the slope of the sensor signal, starts to deviate significantly from the analytical solutions for higher fields, where we are approaching the anisotropy field. It is worth recalling that the small field limit was an approximation we did in Sec. III A. Investigating the transfer curves clearly yields offset-free sensor signals for all theoretical models.

To better understand the sensing performance, we investigate the role of the effective anisotropy $\mu_0 H_k$ and the applied SOT current J_x. First, we vary $\mu_0 H_k$, while keeping the applied current constant at $j_e = 1$ MAcm^{-2}. The sensor signals obtained numerically are illustrated in Fig. 4. We observe that it is possible to modulate both the sensitivity and the linear range of the sensor by changing the anisotropy field. The strength of the effective anisotropy field can be tuned via the thickness of the FM layer (if the PMA originates as an interface effect). In materials such as
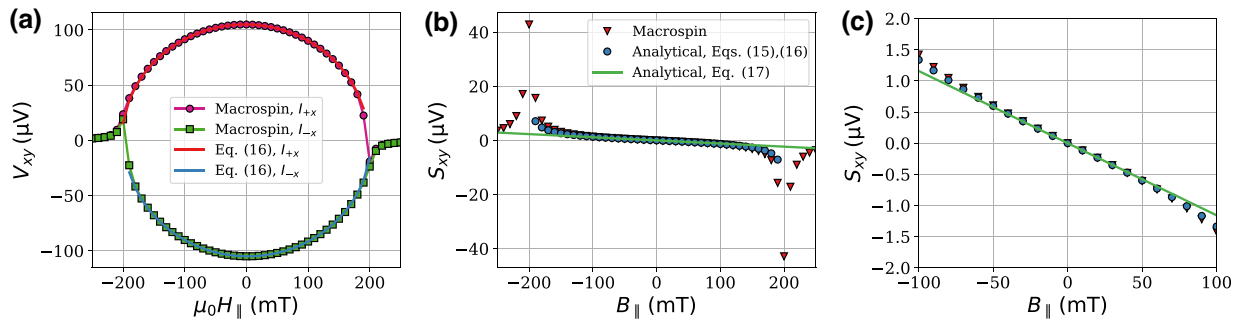

FIG. 3. The simulated (pink, green) and calculated (red, blue) AHE voltages using simple approximation from Eq. (12) are depicted in (a) for both current directions starting from $\mathbf{m}_0 = (0, 0, 1)^T$. The calculated sensor signal is then plotted in (b). Very good agreement between the analytical solutions and the simulations can be observed in the lower field limit, highlighted in (c), which shows an enlarged view of the relevant range.
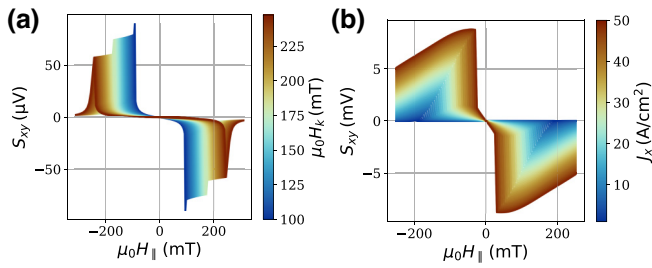
FIG. 4. Dependence of the sensor signal S_{xy} on the strength of the perpendicular magnetic anisotropy is shown in (a), where the linear range increases with $\mu_0 H_k$, but to the cost of the sensitivity. The applied charge current density is depicted in (b), where one can see that a higher current increases the sensitivity of the sensor signal, but, in exchange, it reduces the measurable linear range.

Ta/Co-Fe-B or Pt/Co, which are the materials of choice for SOT investigation, the anisotropy field at room temperature can vary between 50 and 300 mT [5]. On the basis of the desired application, it is possible, in principle, to tune the linear range by either changing materials or adjusting the thickness of the FM layer. Further techniques can be applied to change the effective anisotropies. That is, the annealing or growth temperature will affect not only the SOT parameters but also the effective magnetic anisotropy [40–42]. In the Ta/Co-Fe-B/MgO structures that we consider in our work, variations in the thickness of the FM layer or the thickness of the MgO will result in different PMAs [43]. Furthermore, low-concentration nitrogen doping of Ta can significantly increase PMA [44].

A second measure to tune the sensitivity and linear range of the sensor is the magnitude of the electric current applied to the heavy metal layer; see Fig. 4(b). At higher currents, the magnetization switches much faster into the in-plane state, owing to the stronger current-induced torques, limiting the linear range to be used for magnetic field detection. Higher modulations can be obtained using currents below the switching threshold, leading to an increase in sensitivity. Note that a similar effect could be obtained by changing the material acting as HM in order to scale the exerted torques via the SOT coefficients, or alternative spin polarizing materials can be chosen that use different physics, such as the orbital orbit torque effect [45]. However, the dependence of the sensitivity on the applied current allows us to obtain a magnetic field sensor with tunable sensitivity and linear range. Independent of the chosen parameters, the sensing signal always remains offset-free.

We highlight in Table I the performance prediction for our tunable sensing concept. Assuming that $\mu_0 H_k = 200$ mT, the linear range of the sensor is found to be $\mu_0 H_k = 180$ mT for a low current density regime where $j_e = 1$ MAcm^{-2}, while the sensitivity is rather low (0.017 Ω/T). Thus, a high linear range is obtained at the cost of sensitivity. The product between the linear range and the sensitivity is 0.003 Ω. The sensitivity can be

tuned by increasing the amplitude of the current density. Assuming that $j_e = 50$ MAcm^{-2}, the sensitivity increases to 1.32 Ω/T, but the linear range drops to 15 mT. The product between these two values increases significantly to 0.2 Ω. This is similar to the sensor performance reported by Li *et al.* [21], but the linear range of our concept increases by a factor of 15.

C. Sensor performance

Magnetic field sensors can be best compared with respect to their properties such as linear range, offset, or sensitivity. Therefore, we are interested in the dependence of the linear range and sensitivity on the applied current density J_x and the anisotropy field $\mu_0 H_k$. The latter is a measure of the material used. We numerically simulate with our macrospin model the full sensor transfer curve. We fit this curve with a linear fit around the zero field. The slope defines the sensitivity. The linear range is computed as the field that is required to switch the magnetization, compromising the sensing principle. Figure 5(a) illustrates the dependence of the effective anisotropy chosen and the applied current on the linear measurement range obtained from the magnetic sensor. From Fig. 5, it can be seen that the linear range is very well tunable with changes of $\mu_0 H_k$ and J_x. The sensitivity of the sensor signal depicted in Fig. 5(b) shows two phases. Below a certain given threshold of anisotropy and current, the sensitivity drops significantly, and it cannot be tuned with the current anymore.

The robustness of the sensor against components of the magnetic field that are perpendicular to the measured field direction is another important measure of its performance. Generally, a random magnetic field will have a parallel component $H_\parallel$ that can be projected along the sensitive direction and a perpendicular component $H_\perp$ that is normal to it. The latter can alter the equilibrium state at zero fields, resulting in a decrease in sensor performance.

To investigate the influence of perpendicular perturbation fields ($H_\perp$), we vary the strength of the normal component $H_\perp$, as well as the applied angle θ, which is
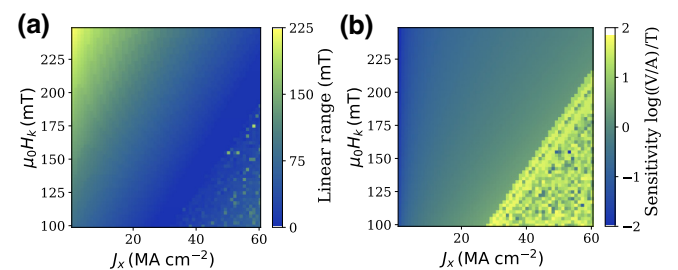

FIG. 5. Magnetic field sensing properties as a function of applied SOT current J_x and effective magnetic anisotropy $\mu_0 H_k$, where the measurable linear range is shown in (a), and the sensitivity is shown in (b).
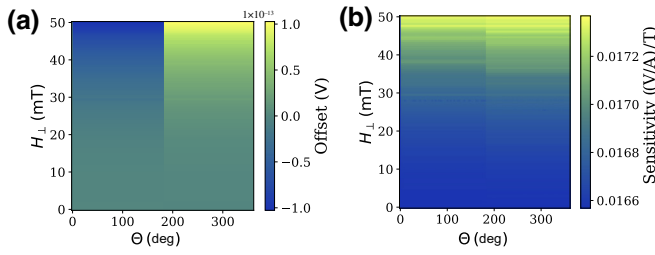
FIG. 6. Influence of the external bias fields on the offset of the sensor signal (a) and on the sensor sensitivity (b). Although in principle the sensor signal remains always offset free, the sensitivity changes slightly, but not significantly, with the amplitude of the perpendicular field $H_\perp$.

the angle between the z axis and the applied field. That is, if $\theta = 0$, then $H_\perp$ is applied parallel to the z axis and if $\theta = \pi/2$ then $H_\perp$ is in the x-y plane. The angle between $H_\perp$ and the equilibrium magnetization is always $\pi/2$.

Figure 6(a) shows that $H_\perp$ does not influence the sensor offset, regardless of the amplitude and angle. Note that if $H_\perp > H_k$ then the magnetization will point along $H_\perp$, compromising the general sensing concept. A weak dependence of the sensitivity on the amplitude of $H_\perp$ and θ can be seen in Fig. 6(b). When the normal field is applied, the sensitivity increases, as the equilibrium state is slightly modulated if positive or negative currents are applied. However, again there exists a threshold $H_\perp < 30$ mT, where the sensitivity of the sensor signal remains rather constant and independent of the angle of magnetization. There is no clear angle dependence.

D. Higher harmonic voltage measurements

To demonstrate the sensor concept developed, we fabricated a Hall cross structure, as explained in Sec. IV. Using the anomalous Hall effect, one can measure the change in m_z. Since our sensor is based on a differential measurement to eliminate the sensing offset, we employ second-harmonic measurements, as discussed in Sec. IV B.
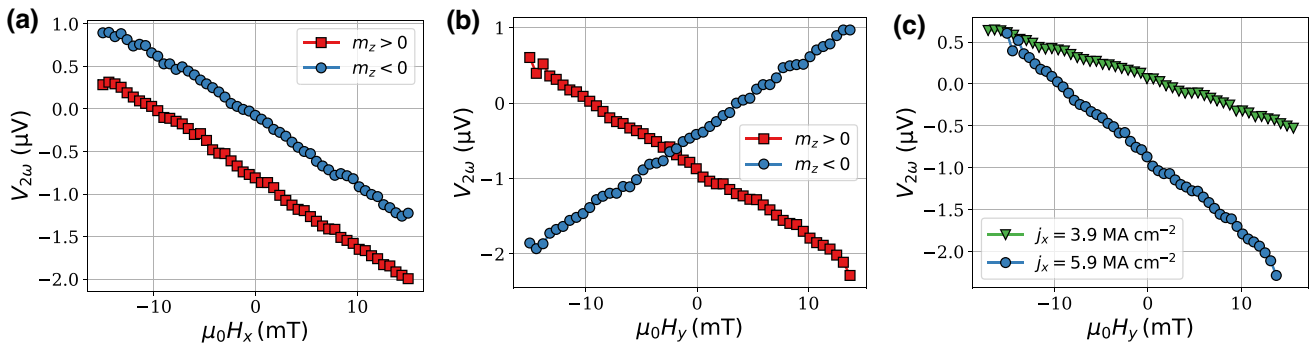
Figure 1(a) illustrates the considered Hall structure. The measured $V_{2\omega}$ curves are plotted as a function of the applied magnetic field in Fig. 7. While the dependence of $V_{2\omega}$ on H_x is given in Fig. 7(a), the dependence of H_y is illustrated in Fig. 7(b). The red (blue) curves show the signal if the sample was presaturated along $+z$ ($-z$) direction using an OOP magnetic field. The charge current density for SOT sensing was $J_x = 28.6$ MAcm^{-2}.

As expected from our simple analytical derivation, as well as from the derivations of Hayashi [37], the 2ω signal should change sign when the magnetic field is applied along the current direction if the initial magnetization state changes sign. If the magnetic field is applied perpendicular to the current direction, that is, H_y, then the slope of the measured signal changes, as shown in Fig. 7.

If one decreases the applied SOT current then the sensitivity of the sensor signal decreases, as theoretically described above and experimentally demonstrated and depicted in Fig. 7(c).

Overall, all signals are linearly dependent on the applied magnetic field, which allows us to experimentally validate the sensor principle using SOT. However, a significant offset is observed if the magnetization is presaturated along the $-z$ direction. In most experimental work in which the HHVA is employed, this offset is usually ignored because the offset does not play a crucial role in the subsequent analysis of the data. This offset is attributed to the measurement setup's electronics. Unfortunately, it limits the sensing performance of our single-device magnetic field sensor. Part of the offset can indeed originate from the measurement setup's electronics. Additionally, this offset can have a more fundamental origin. Since it is very difficult to deposit perfect interfaces, we expect that irregularities on the surface between HM and FM could locally change the material parameters that lead to pinning centers [46] and, thus, to an offset that we do not observe in our numerical investigations. Controlled intermixing at the interfaces will not only increase the Dzyaloshinskii-Moriya interaction, but will create a smoother interface with a lower number

FIG. 7. Experimental results obtained from the second harmonic measurements. In (a) the field parallel to the current direction (H_x) is swept, starting from both magnetization states. The transverse field is swept in (b). The tunable sensitivity can be observed in (c), where we sweep the longitudinal field for the charge current densities $j_e = 3.9$ MAcm^{-2} (green, triangles) and $j_e = 5.9$ MAcm^{-2} (blue, circles).

of defects [47], minimizing this error. However, unwanted intermixing, such as diffusion of B in the Ta layer, leaves behind a crystallized CoFe layer [48] that could show a slightly rotated anisotropy axis. On the same note, Ta can also diffuse into the Co-Fe-B layer, locally changing and varying the anisotropy, thus creating further pinning sites.

The offset can also originate from the anomalous Nernst effect, which contributes to the AHE. With this correction (which do not plot here to show the real measurement data), only a minor offset remains, which we attribute to the system's electronics.

Consider now that current flow in the x direction causes an increase in temperature due to Joule heating. Assuming that the change in temperature is small enough not to alter any material parameters, we expect to have temperature gradients (∇T).

When magnetization **m** and ∇T are normal to each other, then the anomalous Nernst effect (ANE) gives an additional contribution due to the generated electrical field [49]

$$\mathbf{E}_{\mathrm{ANE}} = Q_s \mu_0 M_s (\mathbf{m} \times \nabla T), \qquad (25)$$

where Q_s is the ANE coefficient.

Let us now consider that the temperature gradient has only a z component and we have an arbitrary magnetization state. Thus, the ANE generates an electric field given by

$$\mathbf{E}_{\mathrm{ANE}}(I_{+x}) = Q_s \mu_0 M_s \begin{pmatrix} m_x \\ m_y \\ m_z \end{pmatrix} \times \begin{pmatrix} 0 \\ 0 \\ \partial_z T \end{pmatrix} = \begin{pmatrix} m_y \partial_z T \\ -m_x \partial_z T \\ 0 \end{pmatrix}. \qquad (26)$$

The measured Hall voltage then becomes

$$V_{xy}(I_{+x}) = V_{\mathrm{AHE}}(I_{+x}) + V_{\mathrm{ANE}}(I_{+x}), \qquad (27)$$

where

$$V_{\mathrm{ANE}}(I_{+x}) = wE_y(I_{+x}) = -wQ_s \mu_0 M_s m_x \partial_z T. \qquad (28)$$

For the opposite current, magnetization changes sign for the x and y components, leading to

$$V_{\mathrm{ANE}}(I_{-x}) = wE_y(I_{-x}) = wQ_s \mu_0 M_s m_x \partial_z T. \qquad (29)$$

Summing up the Hall voltages measured for the sensing signal according to Eq. (15) shows that the contributions from the ANE due to $\partial_z T$ are vanishing. Thus, we conclude that the z component of the temperature gradient that originates in the dissipation of Joule heating does not cause any offset.

Let us now consider obtaining a gradient in the temperature where

$$\nabla T = \begin{pmatrix} \partial_x T \\ 0 \\ 0 \end{pmatrix}, \qquad (30)$$

which can originate in the imperfections in current flow and small symmetry distortion, e.g., slightly nonsymmetrical arrangements of vias due to lithography tolerances.

The contribution of ANE to the Hall voltage then becomes

$$V_{\mathrm{ANE}}(I_{+x}) = wE_y(I_{+x}) = wQ_s \mu_0 M_s m_z \partial_x T. \qquad (31)$$

Changing the sign of magnetization leads to the same term,

$$V_{\mathrm{ANE}}(I_{-x}) = wE_y(I_{-x}) = wQ_s \mu_0 M_s m_z \partial_x T, \qquad (32)$$

which leads to the offset $2wQ_s \mu_0 M_s m_z \partial_x T$ when measured voltages are added. These considerations indicate that the nonvanishing offset obtained in the experiments can probably be attributed to ANE. However, this is not due to

(a)

(b)

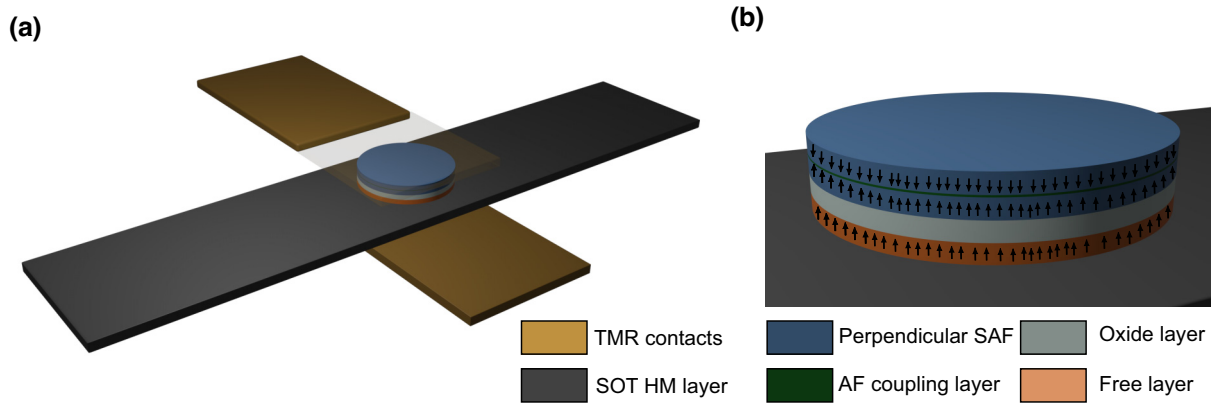|			
TMR contacts	Perpendicular SAF		Oxide layer
SOT HM layer	AF coupling layer		Free layer

FIG. 8. Possible design for a TMR stack for reading out the sensor signal to avoid contributions from ANE and to increase the sensitivity, where the SOT current flows through the HM layer (gray), and the TMR read-out current flows through TMR-contacting layers (gold). The TMR stack consists of a perpendicular synthetic antiferromagnet (blue) antiferromagnetically coupled through a spacer layer (green). The free layer (orange) is separated from the SAF layer by a thin oxide layer (gray).

the z component of the gradient caused by the cooling of the sample toward the heat sink, as originally expected, but due to the broken symmetry of the Hall bar due to fabrication defects, tolerances, or misalignments.

VI. OUTLOOK

The second harmonic measurements performed allowed us to deliver a proof of concept that the proposed sensing method is applicable and second harmonic analysis can be performed to obtain a linear sensing signal. Furthermore, an increase in applied current leads to a higher sensitivity, allowing for the realization of a tunable sensor. However, the experimental validations show that the AHE is not perfectly suitable to measure the change in magnetization, as the anomalous Nernst effect contribution leads to an offset. This additional offset can be eliminated if magnetization is read through a TMR stack [22], as illustrated in Fig. 8. Here, one could make use of a regular HM-FM-oxide tri-layer as the SOT material. A perpendicularly magnetized synthetic antiferromagnetic (SAF) layer is utilized to read the magnetization in the free layer via the TMR effect. Thus, very high sensitivities can be achieved in a range $> k\Omega/T$. The ANE will not be present in the TMR signal; thus, one might probably eliminate the sensing offset we currently observe in our experimental validation.

VII. CONCLUSION

In this work, we propose a novel concept for magnetic field sensing based on spin-orbit torques. The proposed concept is equivalent to the experiments performed to extract the SOT-induced torques, as in the well-established Hayashi method [37].

In this sensing concept, the SOT leads to a symmetric inclination of the initial out-of-plane magnetization for opposite current directions. We investigate the roles of the SOT coefficients η_{damp} and η_{field}, which are a measure of the dampinglike and fieldlike torques, respectively.

Our numerical investigations reveal that the sensor signal evolves linearly with the applied magnetic field in the working regime. This sensing principle shows a large linear range (hundreds of millitesla), whereas the offset vanishes in the absence of an external field. The sensitivity

as well as the linear range can be tuned by varying the amplitude of the charge current and anisotropy fields, respectively.

Perturbation fields applied in the normal plane to the sensitive direction do not affect offset elimination. However, they slightly change the sensitivity of the sensor, and thus lead to poorer sensor performance.

Second harmonic measurements on a Ta/Co-Fe-B/MgO trilayer structured on a Hall cross allowed us to validate the sensing principle, where the sensor signal can be tuned with the applied current. Furthermore, we proposed a TMR stack that will lead to a higher sensitivity and probably eliminate the sensing offset occurred in an AHE device. We believe that our proposed sensing concept will help develop a new generation of sensing devices for accurate absolute field sensing.

The data supporting the findings of this study are available upon reasonable request from the corresponding author.

APPENDIX A: TAYLOR EXPANSION OF THE SENSOR SIGNAL

One can expand Eq. (16) in a Taylor series first at $H_x = 0$, which yields

$$V_{xy}(I_{+x})|_{H_x=0} = \Delta R_{AHE} I_{+x} \sqrt{\frac{-H_{dl}^2 - H_{fl}^2 - 2H_{fl}H_y + H_k^2 - H_y^2}{H_k^2}}$$

$$+ \Delta R_{AHE} I_{+x} H_{dl} H_x \frac{\sqrt{[-H_{dl}^2 - H_{fl}^2 - 2H_{fl}H_y + H_k^2 - H_y^2]/H_k^2}}{H_k^2 \sqrt{1 + [-H_{dl}^2 - (H_{fl} + H_y)^2]/H_k^2}} + \mathcal{O}[H_x]^2. \quad (A1)$$

For the opposite current I_{-x}, we obtain

$$V_{xy}(I_{-x})|_{H_x=0} = \Delta R_{\text{AHE}} I_{-x} \sqrt{-\frac{-H_{\text{dl}}^2 - H_{\text{fl}}^2 + 2H_{\text{fl}}H_y + H_k^2 - H_y^2}{H_k^2}}$$

$$- \Delta R_{\text{AHE}} I_{-x} H_{\text{dl}} H_x \frac{\sqrt{[-H_{\text{dl}}^2 - H_{\text{fl}}^2 + 2H_{\text{fl}}H_y + H_k^2 - H_y^2]/H_k^2}}{-H_{\text{dl}}^2 - H_{\text{fl}}^2 + 2H_{\text{fl}}H_y + H_k^2 - H_y^2} + \mathcal{O}[H_x]^2. \tag{A2}$$

Evaluating Eq. (16) at $H_y = 0$ yields

$$V_{xy}(I_{+x})|_{H_y=0} = \Delta R_{\text{AHE}} I_{+x} \sqrt{-\frac{-H_{\text{dl}}^2 - H_{\text{fl}}^2 + 2H_{\text{dl}}H_x + H_k^2 - H_x^2}{H_k^2}}$$

$$- \Delta R_{\text{AHE}} I_{+x} H_{\text{fl}} H_y \frac{\sqrt{[-H_{\text{dl}}^2 - H_{\text{fl}}^2 + 2H_{\text{dl}}H_x + H_k^2 - H_x^2]/H_k^2}}{-H_{\text{dl}}^2 - H_{\text{fl}}^2 + 2H_{\text{dl}}H_x + H_k^2 - H_x^2} + \mathcal{O}[H_y]^2 \tag{A3}$$

for positive current I_{+x} and

$$V_{xy}(I_{-x})|_{H_y=0} = \Delta R_{\text{AHE}} I_{-x} \sqrt{-\frac{-H_{\text{dl}}^2 - H_{\text{fl}}^2 - 2H_{\text{fl}}H_y + H_k^2 - H_y^2}{H_k^2}}$$

$$+ \Delta R_{\text{AHE}} I_{-x} H_{\text{fl}} H_y \frac{\sqrt{[-H_{\text{dl}}^2 - H_{\text{fl}}^2 - 2H_{\text{fl}}H_y + H_k^2 - H_y^2]/H_k^2}}{H_k^2 \sqrt{1 + [-H_{\text{fl}}^2 - (H_{\text{dl}} + H_x)^2]/H_k^2}} + \mathcal{O}[H_y]^2 \tag{A4}$$

for negative current I_{-x}.

We can then simplify $\sqrt{-(-H_{\text{dl}}^2 - H_{\text{fl}}^2 + 2H_{\text{dl}}H_x + H_k^2 - H_x^2)/H_k^2} \approx 1$, since in the first-order approximation one has to consider $-H_{\text{dl}}^2 - H_{\text{fl}}^2 + 2H_{\text{dl}}H_x - H_x^2 \ll H_k^2$, which leads to even further simplifications, where

$$V_{xy}(I_{+x})|_{H_x=0} = \Delta R_{\text{AHE}} I_0 + \Delta R_{\text{AHE}} I_0 \frac{H_{\text{dl}} Hx}{H_k^2} + \mathcal{O}[H_x]^2, \tag{A5a}$$

$$V_{xy}(I_{-x})|_{H_x=0} = -\Delta R_{\text{AHE}} I_0 + \Delta R_{\text{AHE}} I_0 \frac{H_{\text{dl}} Hx}{H_k^2} + \mathcal{O}[H_x]^2 \tag{A5b}$$

$$V_{xy}(I_{+x})|_{H_y=0} = \Delta R_{\text{AHE}} I_0 - \Delta R_{\text{AHE}} I_0 \frac{H_{\text{fl}} Hy}{H_k^2} + \mathcal{O}[H_y]^2, \tag{A5c}$$

$$V_{xy}(I_{-x})|_{H_y=0} = -\Delta R_{\text{AHE}} I_0 - \Delta R_{\text{AHE}} I_0 \frac{H_{\text{fl}} Hy}{H_k^2} + \mathcal{O}[H_y]^2. \tag{A5d}$$

Summing up all the Taylor expansions, one can then obtain the sensor signal according to Eq. (15).

APPENDIX B: FOURIER EXPANSION OF THE ac SENSOR SIGNAL

The measured time-dependent voltage output $V_{xy}(t)$ upon application of an ac SOT current can be divided into four cases. If one starts with an initial magnetization pointing along [001], i.e., $m_z > 0$, and the magnetic field is applied along the x direction, the AHE voltage is given by

$$V_{xy}(t) = \Delta R_{\text{AHE}} I_0 \sin(\omega t) \sqrt{1 - \frac{(H_x - H_{\text{dl}}(t))^2}{H_k^2}}, \tag{B1}$$

where the current-induced dampinglike torque is now time dependent and becomes

$$H_{\text{dl}}(t) = H_{\text{dl}} \sin(\omega t) \tag{B2}$$

with ω being the frequency of the applied ac current. Thus, one can write Eq. (B1) as

$$V_{xy}(t) = \Delta R_{\mathrm{AHE}} I_0 \sin(\omega t) \cdot \sqrt{1 - \frac{(H_x - H_{\mathrm{dl}} \sin(\omega t))^2}{H_k^2}}.$$
(B3)

Using the approximation $\sqrt{1 - a/b^2} \approx 1 - a/2b^2$ for $(a \ll b^2)$, one can further simplify Eq. (B3) to

$$V_{xy}(t) = \Delta R_{\mathrm{AHE}} I_0 \sin(\omega t)\left(1 - \frac{(H_x - H_{\mathrm{dl}} \sin(\omega t))^2}{2H_k^2}\right).$$
(B4)

The second-order Fourier expansion of Eq. (B4) at ωt can then be written as

$$V_{xy}(t) = \frac{I_0 \Delta R_{\mathrm{AHE}} H_{\mathrm{dl}} H_x}{2H_k{}^2}$$
$$- \frac{I_0 \Delta R_{\mathrm{AHE}}(3H_{\mathrm{dl}}^2 - 8H_k^2 + 4H_x^2)}{8H_k^2} \sin(\omega t)$$
$$- \frac{I_0 \Delta R_{\mathrm{AHE}} H_{\mathrm{dl}} H_x}{2H_k{}^2} \cos(2\omega t).$$
(B5)

Considering that one starts with the opposite magnetization state ($[00\bar{1}]$, $m_z < 0$), the Fourier expansion becomes

$$V_{xy}(t) = \frac{I_0 \Delta R_{\mathrm{AHE}} H_{\mathrm{dl}} H_x}{2H_k{}^2}$$
$$+ \frac{I_0 \Delta R_{\mathrm{AHE}}(3H_{\mathrm{dl}}^2 - 8H_k^2 + 4H_x^2)}{8H_k^2} \sin(\omega t)$$
$$- \frac{I_0 \Delta R_{\mathrm{AHE}} H_{\mathrm{dl}} H_x}{2H_k{}^2} \cos(2\omega t).$$
(B6)

Thus, as a general case, one can then write

$$V_{xy}(t) = \frac{I_0 \Delta R_{\mathrm{AHE}} H_{\mathrm{dl}} H_x}{2H_k{}^2}$$
$$\mp \frac{I_0 \Delta R_{\mathrm{AHE}}(3H_{\mathrm{dl}}^2 - 8H_k^2 + 4H_x^2)}{8H_k^2} \sin(\omega t)$$
$$- \frac{I_0 \Delta R_{\mathrm{AHE}} H_{\mathrm{dl}} H_x}{2H_k{}^2} \cos(2\omega t).$$
(B7)

Analogously, one can derive the Fourier expansion if the magnetic field is applied along the y direction. In this case,

the general form can then be written as

$$V_{xy}(t) = \mp \frac{I_0 \Delta R_{\mathrm{AHE}} H_{\mathrm{fl}} H_y}{2H_k{}^2}$$
$$\mp \frac{I_0 \Delta R_{\mathrm{AHE}}(3H_{\mathrm{fl}}^2 - 8H_k^2 + 4H_y^2)}{8H_k^2} \sin(\omega t)$$
$$\pm \frac{I_0 \Delta R_{\mathrm{AHE}} H_{\mathrm{fl}} H_y}{2H_k{}^2} \cos(2\omega t).$$
(B8)

Considering both initial magnetization states, as well as the different applied magnetic fields, a general equation of $V_{xy}(t)$ can be given:

$$V_{xy}(t) = \frac{I_0 \Delta R_{\mathrm{AHE}}(H_{\mathrm{dl}} H_x \mp H_{\mathrm{fl}} H_y)}{2H_k{}^2}$$
$$\mp \frac{I_0 \Delta R_{\mathrm{AHE}}(3(H_{\mathrm{dl}}^2 + H_{\mathrm{fl}}^2) - 16H_k^2 + 4(H_x^2 + H_y^2))}{8H_k^2}$$
$$\times \sin(\omega t)$$
$$- \frac{I_0 \Delta R_{\mathrm{AHE}}(H_{\mathrm{dl}} H_x \mp H_{\mathrm{fl}} H_y)}{2H_k{}^2} \cos(2\omega t).$$
(B9)

[1] M. Baibich, J. Broto, A. Fert, F. Van Dau, F. Petroff, P. Eitenne, G. Creuzet, A. Friederich, and J. Chazelas, Giant magnetoresistance of (001)Fe/(001)Cr magnetic superlattices, Phys. Rev. Lett. **61,** 2472 (1988).

[2] G. Binasch, P. Grünberg, F. Saurenbach, and W. Zinn, Enhanced magnetoresistance in layered magnetic structures with antiferromagnetic interlayer exchange, Phys. Rev. B **39,** 4828 (1989).

[3] S. Zhang, P. M. Levy, and A. Fert, Mechanisms of spin-polarized current-driven magnetization switching, Phys. Rev. Lett. **88,** 236601 (2002).

[4] J. C. Slonczewski, Current-driven excitation of magnetic multilayers, J. Magn. Magn. Mater. **159,** L1 (1996).

[5] A. Manchon, J. Železný, I. Miron, T. Jungwirth, J. Sinova, A. Thiaville, K. Garello, and P. Gambardella, Current-induced spin-orbit torques in ferromagnetic and antiferromagnetic systems, Rev. Mod. Phys. **91,** 035004 (2019).

[6] S. Bader and S. Parkin, Spintronics, Annu. Rev. Condens. Matter Phys. **1,** 71 (2010).

[7] S. Bhatti, R. Sbiaa, A. Hirohata, H. Ohno, S. Fukami, and S. Piramanayagam, Spintronics based random access memory: A review, Mater. Today **20,** 530 (2017).

[8] Q. Shao, P. Li, L. Liu, H. Yang, S. Fukami, A. Razavi, H. Wu, K. Wang, F. Freimuth, Y. Mokrousov, M. D. Stiles, S. Emori, A. Hoffmann, J. Åkerman, K. Roy, J.-P. Wang, S.-H. Yang, K. Garello, and W. Zhang, Roadmap of spin—orbit torques, IEEE Trans. Magn. **57,** 1 (2021).

[9] A. V. Chumak, *et al.*, Advances in magnetics roadmap on spin-wave computing, IEEE Trans. Magn. **58,** 1 (2022).

[10] I. M. Miron, K. Garello, G. Gaudin, P.-J. Zermatten, M. V. Costache, S. Auffret, S. Bandiera, B. Rodmacq, A. Schuhl, and P. Gambardella, Perpendicular switching of a single

ferromagnetic layer induced by in-plane current injection, Nature **476**, 189 (2011).

[11] K. Garello, C. O. Avci, I. M. Miron, M. Baumgartner, A. Ghosh, S. Auffret, O. Boulle, G. Gaudin, and P. Gambardella, Ultrafast magnetization switching by spin-orbit torques, Appl. Phys. Lett. **105**, 212402 (2014).

[12] M. Cubukcu, O. Boulle, M. Drouard, K. Garello, C. Onur Avci, I. Mihai Miron, J. Langer, B. Ocker, P. Gambardella, and G. Gaudin, Spin-orbit torque magnetization switching of a three-terminal perpendicular magnetic tunnel junction, Appl. Phys. Lett. **104**, 042406 (2014).

[13] C. Zhang, S. Fukami, H. Sato, F. Matsukura, and H. Ohno, Spin-orbit torque induced magnetization switching in nano-scale Ta/CoFeB/MgO, Appl. Phys. Lett. **107**, 012401 (2015).

[14] C. O. Avci, A. Quindeau, C.-F. Pai, M. Mann, L. Caretta, A. S. Tang, M. C. Onbasli, C. A. Ross, and G. S. D. Beach, Current-induced switching in a magnetic insulator, Nat. Mater. **16**, 309 (2017).

[15] I. M. Miron, T. Moore, H. Szambolics, L. D. Buda-Prejbeanu, S. Auffret, B. Rodmacq, S. Pizzini, J. Vogel, M. Bonfim, A. Schuhl, and G. Gaudin, Fast current-induced domain-wall motion controlled by the Rashba effect, Nat. Mater. **10**, 419 (2011).

[16] W. Jiang, G. Chen, K. Liu, J. Zang, S. G. Te Velthuis, and A. Hoffmann, Skyrmions in magnetic multilayers, Phys. Rep. **704**, 1 (2017).

[17] K. Everschor-Sitte, J. Masell, R. M. Reeve, and M. Kläui, Perspective: Magnetic skyrmions—overview of recent progress in an active research field, J. Appl. Phys. **124**, 240901 (2018).

[18] L.-M. Kern, *et al.*, Deterministic generation and guided motion of magnetic skyrmions by focused He$^+$-ion irradiation, Nano Lett. **22**, 4028 (2022).

[19] S. Vélez, S. Ruiz-Gómez, J. Schaab, E. Gradauskaite, M. S. Wörnle, P. Welter, B. J. Jacot, C. L. Degen, M. Trassin, M. Fiebig, and P. Gambardella, Current-driven dynamics and ratchet effect of skyrmion bubbles in a ferrimagnetic insulator, Nat. Nanotechnol. **17**, 834 (2022).

[20] Y. Xu, Y. Yang, M. Zhang, Z. Luo, and Y. Wu, Ultrathin all-in-one spin hall magnetic sensor with built-in AC excitation enabled by spin current, Adv. Mater. Technol. **3**, 1800073 (2018).

[21] R. Li, S. Zhang, S. Luo, Z. Guo, Y. Xu, J. Ouyang, M. Song, Q. Zou, L. Xi, X. Yang, J. Hong, and L. You, A spin—orbit torque device for sensing three-dimensional magnetic fields, Nat. Electron. **4**, 179 (2021).

[22] D. Suess, U. Ausserlechner, and A. Satz, Device and method for detecting a magnetic field using the spin orbit torque effect, US Patent App. 17/220,129, (2021).

[23] J. Heremans, Solid state magnetic field sensors and applications, J. Phys. D: Appl. Phys. **26**, 1149 (1993).

[24] D. L. Graham, H. A. Ferreira, and P. P. Freitas, Magnetoresistive-based biosensors and biochips, Trends Biotechnol. **22**, 455 (2004).

[25] I. R. McFadyen, E. E. Fullerton, and M. J. Carey, State-of-the-art magnetic hard disk drives, MRS Bull. **31**, 379 (2006).

[26] D. Suess, A. Bachleitner-Hofmann, A. Satz, H. Weitensfelder, C. Vogler, F. Bruckner, C. Abert, K. Prügl, J. Zimmer, C. Huber, S. Luber, W. Raberg, T. Schrefl, and

H. Brückl, Topologically protected vortex structures for low-noise magnetic sensors with high linear range, Nat. Electron. **1**, 362 (2018).

[27] T. Zhu, P. Chen, Q. H. Zhang, R. C. Yu, and B. G. Liu, Giant linear anomalous Hall effect in the perpendicular CoFeB thin films, Appl. Phys. Lett. **104**, 202404 (2014).

[28] W. L. Peng, J. Y. Zhang, L. S. Luo, G. N. Feng, and G. H. Yu, The ultrasensitive anomalous Hall effect induced by interfacial oxygen atoms redistribution, J. Appl. Phys. **125**, 093906 (2019).

[29] K. Wang, Y. Zhang, and G. Xiao, Anomalous Hall sensors with high sensitivity and stability based on interlayer exchange-coupled magnetic thin films, Phys. Rev. Appl. **13**, 064009 (2020).

[30] J. E. Hirsch, Spin Hall effect, Phys. Rev. Lett. **83**, 1834 (1999).

[31] K. Garello, I. M. Miron, C. O. Avci, F. Freimuth, Y. Mokrousov, S. Blügel, S. Auffret, O. Boulle, G. Gaudin, and P. Gambardella, Symmetry and magnitude of spin—orbit torques in ferromagnetic heterostructures, Nat. Nanotech. **8**, 587 (2013).

[32] Allegro Hall sensor a1304, https://www.allegromicro.com/en/products/sense/linear-and-angular-position/linear-position-sensor-ics/a1304.

[33] T. Gilbert, A phenomenological theory of damping in ferromagnetic materials, IEEE Trans. Magn. **40**, 3443 (2004).

[34] C. Abert, Micromagnetics and spintronics: Models and numerical methods, Eur. Phys. J. B **92**, 120 (2019).

[35] J. C. Slonczewski, Currents and torques in metallic magnetic multilayers, J. Magn. Magn. Mater. **247**, 324 (2002).

[36] C. Abert, H. Sepehri-Amin, F. Bruckner, C. Vogler, M. Hayashi, and D. Suess, Fieldlike and dampinglike spin-transfer torque in magnetic multilayers, Phys. Rev. Appl. **7**, 054007 (2017).

[37] M. Hayashi, J. Kim, M. Yamanouchi, and H. Ohno, Quantitative characterization of the spin-orbit torque using harmonic Hall voltage measurements, Phys. Rev. B **89**, 144425 (2014).

[38] T. Schulz, K. Lee, B. Krüger, R. L. Conte, G. V. Karnad, K. Garcia, L. Vila, B. Ocker, D. Ravelosona, and M. Kläui, Effective field analysis using the full angular spin-orbit torque magnetometry dependence, Phys. Rev. B **95**, 224409 (2017).

[39] F. Bruckner, S. Koraltan, C. Abert, and D. Suess, magnum.np − a pytorch based gpu enhanced finite difference micromagnetic simulation framework for high level development and inverse design, ArXiv:2302.08843 (2023).

[40] Y. Liu, L. Hao, and J. Cao, Effect of annealing conditions on the perpendicular magnetic anisotropy of Ta/CoFeB/MgO multilayers, AIP Adv. **6**, 045008 (2016).

[41] H. Meng, W. Lum, R. Sbiaa, S. Lua, and H. Tan, Annealing effects on CoFeB-MgO magnetic tunnel junctions with perpendicular anisotropy, J. Appl. Phys. **110**, 033904 (2011).

[42] C. O. Avci, K. Garello, C. Nistor, S. Godey, B. Ballesteros, A. Mugarza, A. Barla, M. Valvidares, E. Pellegrin, and A. Ghosh, *et al.*, Fieldlike and antidamping spin-orbit torques in as-grown and annealed Ta/CoFeB/MgO layers, Phys. Rev. B **89**, 214419 (2014).

[43] C.-W. Cheng, W. Feng, G. Chern, C. Lee, and T.-h. Wu, Effect of cap layer thickness on the perpendicular magnetic

anisotropy in top MgO/CoFeB/Ta structures, J. Appl. Phys. **110**, 033916 (2011).

[44] J. Sinha, M. Hayashi, A. J. Kellock, S. Fukami, M. Yamanouchi, H. Sato, S. Ikeda, S. Mitani, S.-h. Yang, and S. S. Parkin, *et al.*, Enhanced interface perpendicular magnetic anisotropy in Ta— CoFeB— MgO using nitrogen doped Ta underlayers, Appl. Phys. Lett. **102**, 242405 (2013).

[45] S. Ding, A. Ross, D. Go, L. Baldrati, Z. Ren, F. Freimuth, S. Becker, F. Kammerbauer, J. Yang, G. Jakob, Y. Mokrousov, and M. Kläui, *et al.*, Harnessing orbital-to-spin conversion of interfacial orbital currents for efficient spin-orbit torques, Phys. Rev. Lett. **125**, 177201 (2020).

[46] C. Burrowes, N. Vernier, J.-P. Adam, L. Herrera Diez, K. Garcia, I. Barisic, G. Agnus, S. Eimer, J.-V. Kim, and T. Devolder, *et al.*, Low depinning fields in Ta-CoFeB-MgO

ultrathin films with perpendicular magnetic anisotropy, Appl. Phys. Lett. **103**, 182401 (2013).

[47] L. H. Diez, M. Voto, A. Casiraghi, M. Belmeguenai, Y. Roussigné, G. Durin, A. Lamperti, R. Mantovan, V. Sluka, and V. Jeudy, *et al.*, Enhancement of the Dzyaloshinskii-Moriya interaction and domain wall velocity through interface intermixing in Ta/CoFeB/MgO, Phys. Rev. B **99**, 054431 (2019).

[48] J. Sinha, M. Gruber, M. Kodzuka, T. Ohkubo, S. Mitani, K. Hono, and M. Hayashi, Influence of boron diffusion on the perpendicular magnetic anisotropy in Ta— CoFeB— MgO ultrathin films, J. Appl. Phys. **117**, 043913 (2015).

[49] M. Mizuguchi and S. Nakatsuji, Energy-harvesting materials based on the anomalous Nernst effect, Sci. Technol. Adv. Mater. **20**, 262 (2019).